UCRL- 91120
PREPRINT

PLASMA MODELING OF MFTF-B AND THE SENSITIVITY TO VACUUM CONDITIONS

G. D. Porter and M. Rensink

This Paper Was Prepared For Submittal To
31st National Vacuum Symposium
MGM Grand Hotel, Reno, Nevada, Dec. 4-7, 1984

September 12, 1984

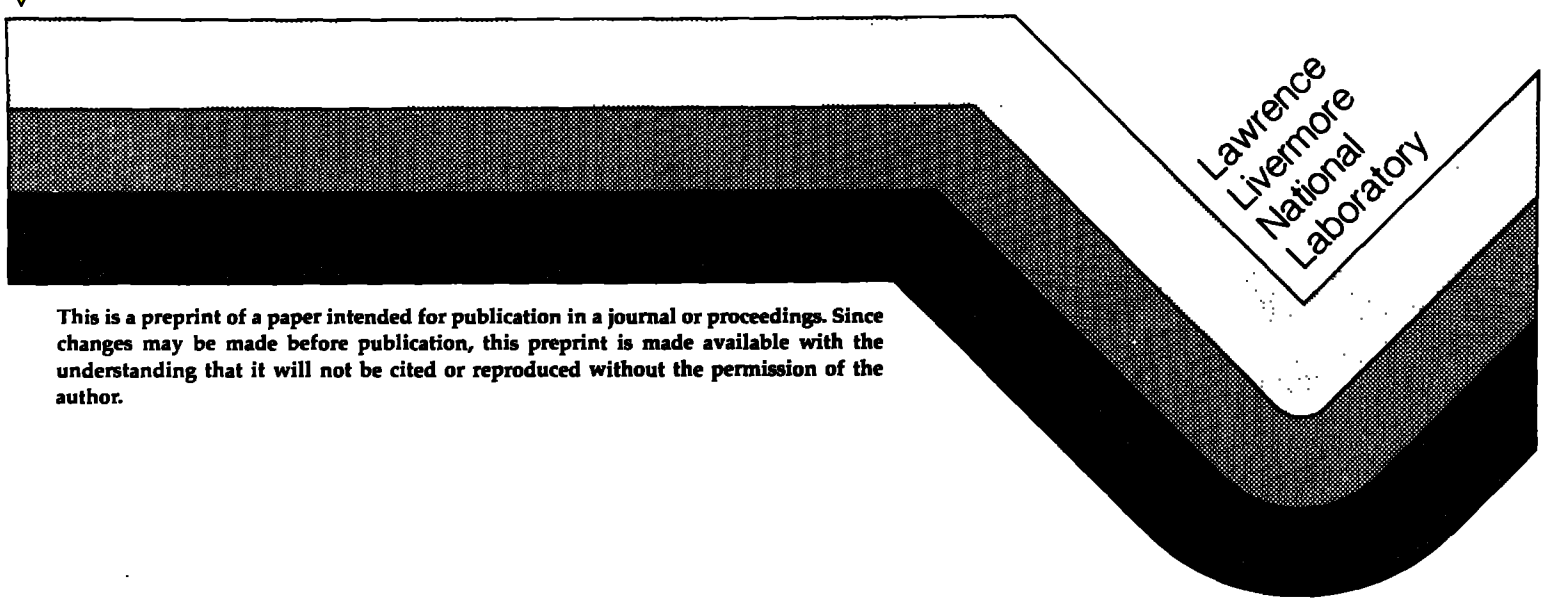

PLASMA MODELING OF MFTF-B AND THE SENSITIVITY TO VACUUM CONDITIONS*

G. D. Porter and M. Rensink
Lawrence Livermore National Laboratory, University of California
Livermore, CA 94550

The Mirror Fusion Test Facility (MFTF-B) is a large tandem mirror device currently under construction at Lawrence Livermore National Laboratory. The completed facility will consist of a large variety of components. Specifically, the vacuum vessel that houses the magnetic coils is basically a cylindrical vessel 60 m long and 11 m in diameter. The magnetics system consists of some 28 superconducting coils, each of which is located within the main vacuum vessel. Twenty of these coils are relatively simple solenoidal coils, but the remaining eight are of a more complicated design to provide an octupole component to certain regions of the magnetic field. The vacuum system is composed of a rough vacuum chain, used to evacuate the vessel from atmospheric pressure, and a high vacuum system, used to maintain good vacuum conditions during a plasma shot. High vacuum pumping is accomplished primarily by cryogenic panels cooled to 4.5 K. Details of this vacuum system has been reported previously.[1]

The MFTF-B coil set is shown in Fig. 1 together with typical axial profiles of magnetic field (a), electrostatic potential (b), and plasma density (c). The plasma is divided into nine regions axially, as labelled on the coil set in Fig. 1. The central cell, which is completely azimuthally symmetric, contains a large volume plasma that is confined by a combination of the magnetic fields and the electrostatic potentials in the yin-yang cell.

*Work performed under the auspices of the U.S. Department of Energy by the Lawrence Livermore National Laboratory under contract number W-7405-ENG-48.

Although not shown in Fig. 1, the axicell can be made to be a simple magnetic well by increasing the current in the large coil at the end of the central cell. Such a configuration can be utilized on MFTF-B, but it is not considered to be the primary configuration. In the primary configuration, depicted in Fig. 1, the axicell is simply an extension of the central cell. The transition cell contains the two coils that are required to make the transition from circular flux tubes at the end of the axicell to highly elliptical flux tubes at the inner end of the yin-yang cell. These elliptical flux tubes are created by the quadrupole nature of the yin-yang coil set. The yin-yang cell is sometimes referred to as the anchor because the quadrupole nature of the magnetic field in that cell provides the stability against magnetohydrodynamic (MHD) modes for the whole machine; i.e., it acts as an anchor against gross plasma motion across the magnetic field.

As shown in curve (b) of Fig. 1, there are both a local potential minimum and an absolute potential maximum in each yin-yang cell. These two features--key to the particle confinement of the machine--are created by the application of neutral beams and electron-cyclotron resonant heating (ECRH) in that cell. The neutral beams are injected in such a way that the density of the high energy ions produced from that beam peaks off the midplane of the yin-yang cell. The beams are injected off the midplane of the cell, and the ions are accelerated toward the center by the magnetic field gradient. After passing the midplane, the ions are decelerated by the field gradient until their axial velocity goes to zero and they are turned around. The density maximum occurs at these turning points, and the ions are thus called the sloshing ions.

Each of the density maxima creates a local region in which electrons are electrostatically confined. The potential maximum on the outboard side of the

yin-yang cell is created by applying ECRH in the region of these electrostatically confined electrons. This potential maximum is referred to as the ion plug, or simply the plug, because it electrostatically stoppers the flow of ions from the central cell.

The rf waves heat the electrons, driving them out of the potential well, and the potential increases to provide a neutral plasma. The potential minimum at the midplane of the yin-yang cell is created by a combination of pumping to remove cold ions in that region and ECRH to enhance the confinement of electrons there. For this purpose, the electron heating is applied near the midplane, heats the electron component that is magnetically confined by the yin-yang magnets, and so enhances their lifetime in that cell. This potential minimum is referred to as a thermal barrier[2] because it thermally isolates the electrons in the central cell from those confined in the ion plug region. It is this thermal barrier that permits operation with central cell densities which are higher than those in the anchor [see curve (c) of Fig. 1].

Modeling of the plasma performance in this configuration must take into account the interaction of plasmas in all regions of the machine. For example, central cell ions scatter until their pitch angle permits them to reach the yin-yang cell where they are reflected by the plug potential. The scattering that occurs while in the yin-yang cell will trap those ions there, creating a cold plasma component in the thermal barrier. The scattering rate, and hence the filling rate of this population, depends on the density and temperature of the central cell ions.[3] Similarly, the potential profile, and hence the confinement time of central cell particles, depends in detail on the neutral beam currents, ECRH powers, and cold neutral densities in the yin-yang cell. Therefore, the plasma model must consist of coupled equations that reflect particle populations in each cell.

We have developed such a model to describe the time evolution of particle density and energy of seven plasma species in three separate machine cells; however, this model does not yet permit analysis of the machine with the axicell run as a separate cell. We have incorporated the interaction with eight neutral species, including cold gas and neutral beams. Although this model has been described elsewhere,[4] briefly it represents plasma species in each cell by a set of zero-dimensional rate equations for density and energy. In general, we do not include radial effects. We do, however, attempt a crude model for radial neutral gas attenuation in the central cell.

We have applied this plasma model to a study of the startup of the MFTF-B plasma. An example of the output from the code is illustrated in Fig. 2, which shows the time evolution of the sloshing-ion density and the cold ion density in the yin-yang cell for two values of neutral gas density in the anchor. In Fig. 2a the anchor neutral gas density (at the plasma core) is assumed to be 10^7 molecules/cm^3, and in Fig. 2b it is assumed to be 2×10^8 molecules/cm^3. This calculation simulates the conditions that are expected to exist during the first 0.5 s of the plasma shot. During this startup phase, there are three neutral beam sources used for the production of the anchor sloshing-ion population. After 0.5 s, two of these sources are turned off and a single, long-pulse source is used to sustain the sloshing ions. There is also one neutral beam (a pump beam) that is used to pump out cold ions in the thermal barrier. This pump beam also removes sloshing ions, preventing pitch-angle scattering of the hot ions. Hence, it permits the maintenance of the sloshing-ion distribution.

During the initial 25 ms of the pulse, the warm ion trapping rate is very rapid. This effect, which can be seen from the dramatic build-up of their density in Fig. 2, occurs because the central cell density is escalating

fairly rapidly but there is not enough power to obtain a high temperature. The scattering rate of the passing ions varies inversely with their temperature; hence, these low temperature ions scatter quickly and fill in the barrier. To avoid this problem, we apply about 300 kW of ICRH power to the central cell ions, starting at 25 ms. As can be seen in Fig. 2, the trapping rate of the warm ions drops rapidly after the application of this ICRH, and the pump beam can adequately control the warm ion density.

As depicted in Fig. 2, the sloshing-ion density that can be achieved with high-anchor neutral-gas density is only about one-fourth of that which can be obtained with low gas density. The reason for this behavior can be understood by considering Fig. 3. This figure shows the magnitude of the sloshing-ion sources and losses for the buildup shown in Fig. 2. The dominant source term for both low neutral gas density (Fig. 3a) and high gas density (Fig. 3b) is ionization of the sloshing-ion neutral beams by the sloshing-ion population. This term is labeled (1) in Fig. 3. Other sources, such as charge-exchange between the beam and the passing ions (5) or charge-exchange between the beam and warm trapped ions (3), are significantly smaller. The dominant loss term in both cases is the charge-exchange losses by the pump beam (loss term 9). With low neutral-gas density, the losses created by charge-exchange between the sloshing ions and gas (10) are almost a factor of 30 lower than the losses on the pump beam. However, with higher gas density, these losses are only a factor of 2 below the pump beam losses.

Note that all of the source terms and loss terms discussed above depend linearly on the sloshing-ion density. The equilibrium density of the sloshing ions is determined by balancing these linear processes with the nonlinear loss mechanism of self-scattering (11). Thus, although the losses created by charge-exchange on the gas never get to be more than one-half of the dominant

loss mechanism, the sloshing-ion density decreases by a factor of one-fourth from the increase in the anchor neutral gas density. The dependence of the sloshing-ion density on the neutral gas density is shown in Fig. 4.

Calculations such as those discussed above have permitted us to determine the maximum neutral-gas densities that are consistent with successful operation of MFTF-B. These density limits are summarized in Table 1 for both startup and steady state conditions. The gas densities shown in this table represent the maximum density on the axis of the machine. The allowed vacuum pressure in each region of the machine is then determined by calculating the gas attenuation in the plasma.

As expected, the vacuum requirements are somewhat more stringent at steady state than during startup. This occurs because more neutral beam power is available during startup. The one exception to this is the allowed gas densities in the end cells. In this case, the limitation on the gas is the buildup of a cold plasma density in the end cell. This cold plasma permits a higher emission rate of secondary electrons off the end plate.[5] These secondary electrons, in turn, increase the power losses through the electrons. Overall, this process is relatively insensitive to the neutral beam heating.

Table 1. Neutral density limits in the MFTF-B plasma core.

	Startup ($t < 0.5$ s)		Steady state ($0.5 < t < 30$ s)	
Region	Density	Limitation	Density	Limitation
Central cell	2×10^7	Hot ion loss rate	7×10^6	Hot ion loss rate
Transition/ Anchor	4×10^7	Hot ion loss rate	1×10^7	Hot ion loss rate
End cell	5×10^{10}	Secondary electrons	5×10^{10}	Secondary electrons

REFERENCES

1. Margolies, D. S. and Valby, L. E., "The Changing MFTF Vacuum Environment," Journal of Vacuum Science & Technology A 1, No. 2, 1308 April-June, 1983.

2. Baldwin, D. E. and Logan, B. G., "Improved Tandem Mirror Fusion Reactor," Phys. Rev Lett. 43, 1318.

3. Futch, A. H. and LoDestro, L. L., Collisional Trapping Rates for Ions in a Magnetic and Potential Well, Lawrence Livermore National Laboratory, Livermore, CA, Report UCRL-87249 (1982).

4. Rensink, M. E., A Model Distribution Function for Thermal Barrier Electrons, Lawrence Livermore National Laboratory, Livermore, CA, Report UCRL-90453 (1984).

5. Porter, G. D., "Effect of Gas Recycling and Secondary Electron Emission on Axial Power Flow in and Open-Ended Device," Nucl. Fusion 22, 1279 (1982).

FIGURE CAPTIONS

1. The MFTF-B magnet configuration and axial profiles of magnetic field, electrostatic potential, and plasma density.

2. The time-dependent behavior of the anchor ion densities in MFTF-B. Figure (a) shows the evolution of the warm ion and sloshing densities with the anchor neutral density of 1×10^7 molecules/cm^3, and Fig. (b) shows the behavior with a neutral density of 2×10^8 molecules/cm^3.

3. The time dependence of the source and loss terms for the anchor sloshing-ion population under the same conditions as in Fig. 2. The source terms are shown as solid lines, and losses are shown as dotted lines. The source terms, which originate from interaction with the sloshing-ion neutral beams, are: ionization by the sloshing ions (1), ionization by warm trapped ions (2), charge-exchange on warm trapped ions (3), ionization by passing ions (4), charge-exchange on passing ions (5), and ionization by hot electrons (8). The loss terms are: charge-exchange on the pump beam (9), charge-exchange on neutral gas (10), and self-scattering (11).

4. The dependence of the anchor sloshing-ion density on the neutral gas density.

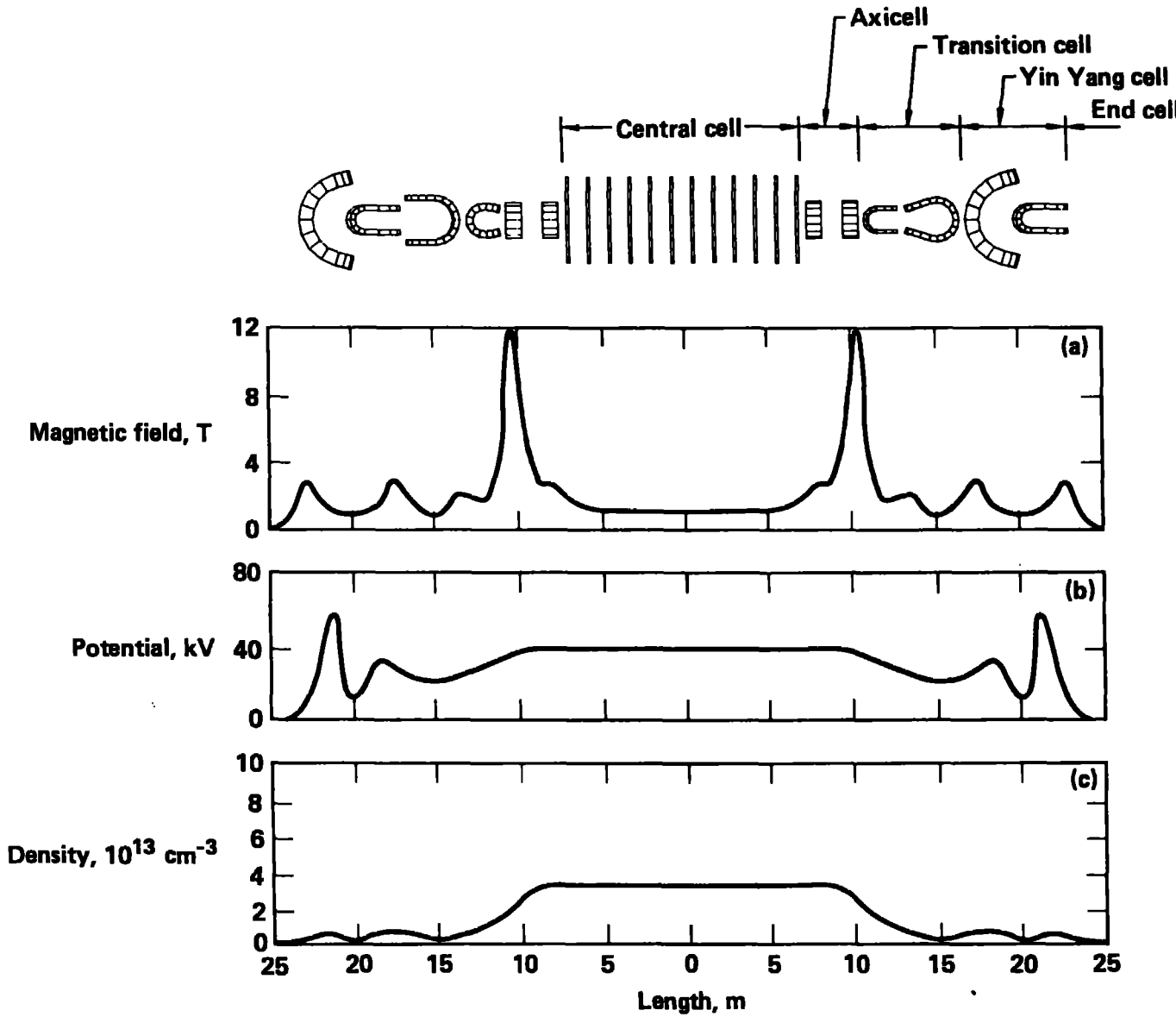
Axicell
Transition cell
Yin Yang cell
End cell
Central cell
Magnetic field, T
12
8
4
0
(a)
Potential, kV
80
40
0
(b)
Density, 10^{13} cm^{-3}
10
8
6
4
2
0
(c)
25
20
15
10
5
0
5
10
15
20
25
Length, m

Fig. 1.

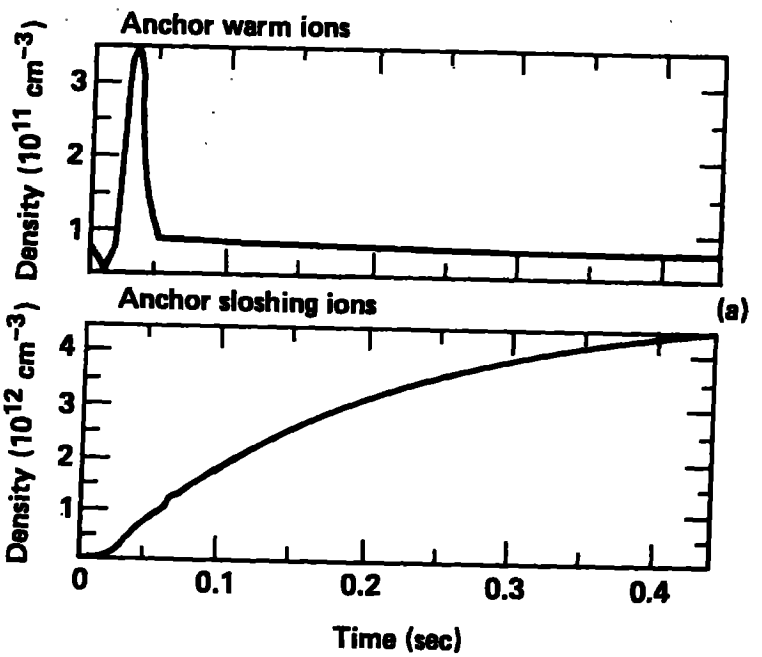
Anchor warm ions
Density (10^{11} cm^{-3})
3
2
1
Anchor sloshing ions
(a)
Density (10^{12} cm^{-3})
4
3
2
1
0
0.1
0.2
0.3
0.4
Time (sec)

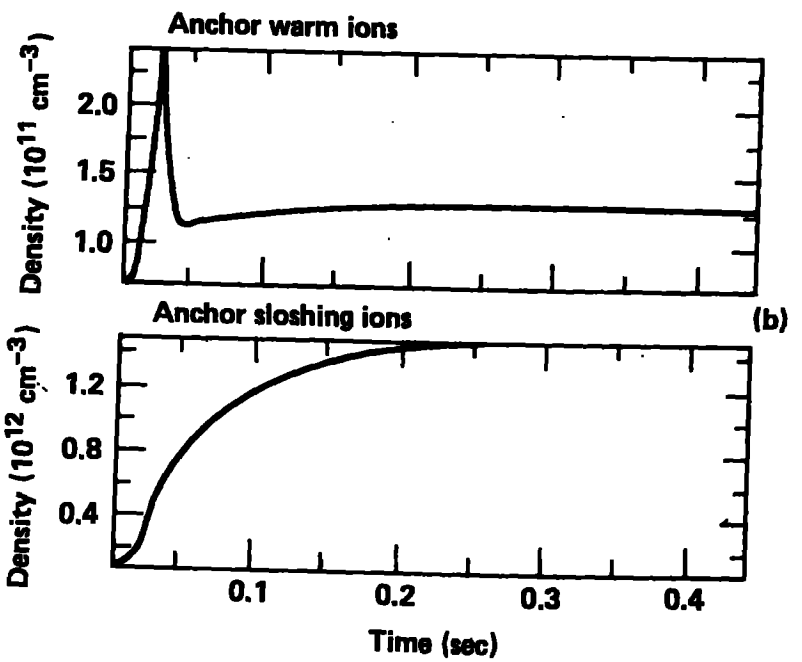
Anchor warm ions
Density (10^{11} cm^{-3})
2.0
1.5
1.0
Anchor sloshing ions
(b)
Density (10^{12} cm^{-3})
1.2
0.8
0.4
0.1
0.2
0.3
0.4
Time (sec)

Fig. 2.

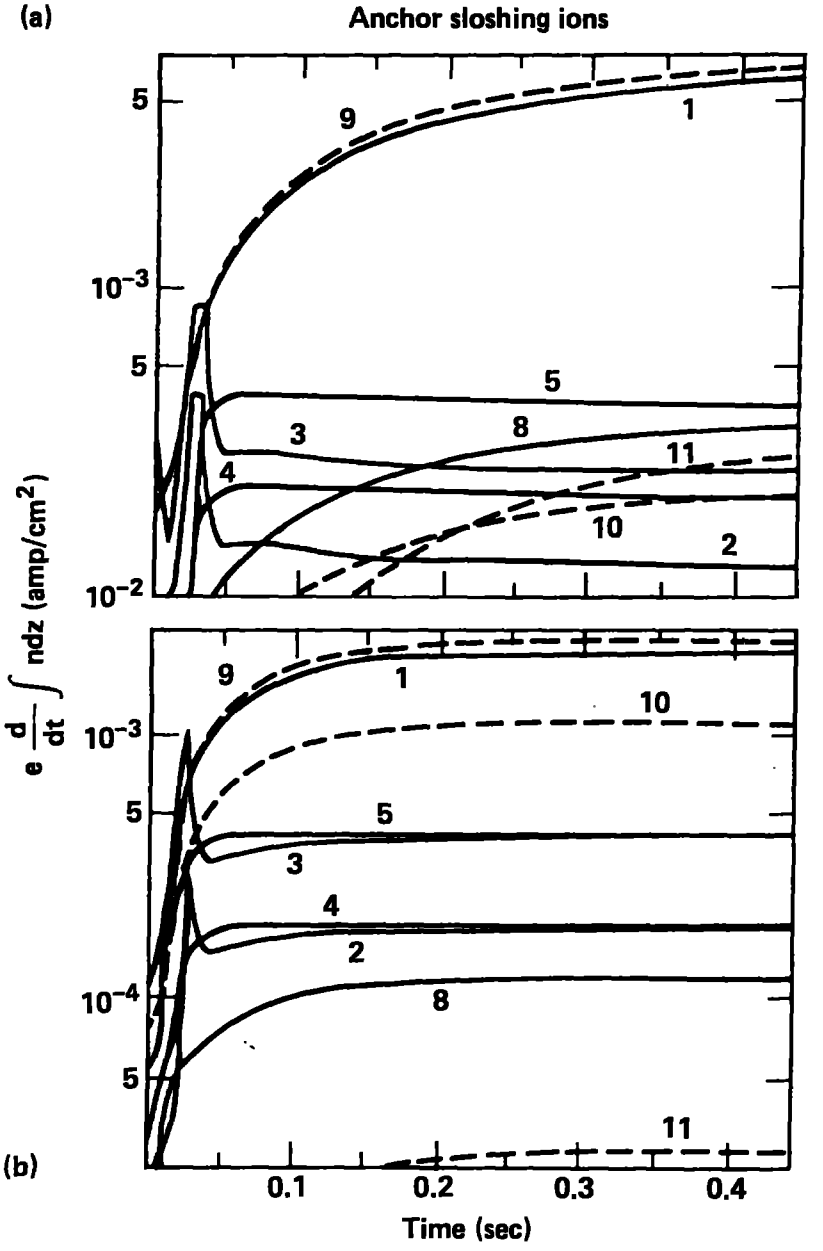
(a)
Anchor sloshing ions
5
10^{-3}
5
10^{-2}
9
1
5
3
8
11
4
10
2
$e\frac{d}{dt}\int ndz$ (amp/cm^2)
9
1
10
10^{-3}
5
5
3
4
2
10^{-4}
8
5
11
(b)
0.1
0.2
0.3
0.4
Time (sec)

Fig. 3.

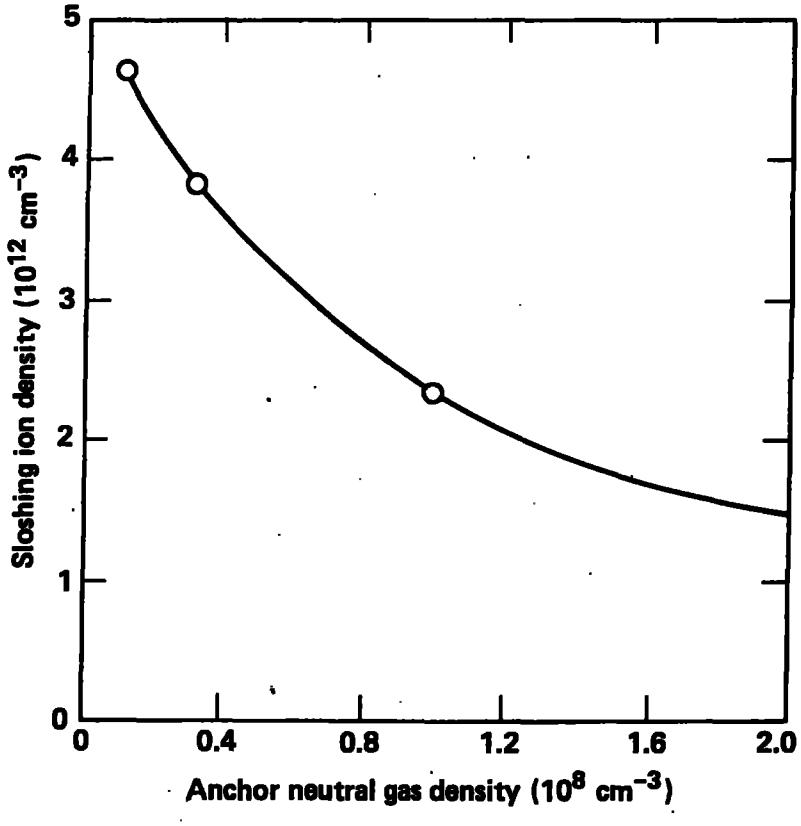
Sloshing ion density (10^{12} cm^{-3})
5
4
3
2
1
0
0
0.4
0.8
1.2
1.6
2.0
Anchor neutral gas density (10^{8} cm^{-3})

Fig. 4.